Direct Calculations of Plume Dynamics of a Pulse Detonation Engine by the CE/SE Method

Zeng-Chan Zhang[1] S.T. John Yu[2] Hao He[3]
Wayne State University
Detroit, MI 48202
www.cfd.eng.wayne.edu

Philip C. E. Jorgenson[4]
NASA Glenn Research Center
Cleveland, OH 44135
www.grc.nasa.gov/WWW/microbus/index.html

Abstract

This paper reports preliminary numerical results of plume dynamics for a pulse detonation engine (PDE). The space-time CE/SE method was used to solve the two-dimensional and axisymmetric Euler equations in conjunction with one chemical species equation in a time-accurate manner. Chemical reactions are simulated by a one-step, irreversible, finite rate model. The stiff source term in the species equation is treated by a point-wise implicit method based on a space-time volumetric integration of the source term over each CE. Numerical results show complex vortex/shock interactions in the vicinity of the thruster exit. Away from the PDE tube, spherical expansion of sound waves is evident. Although a much finer mesh will be needed to further resolve the relevant flow physics, the present results provide an encouraging first step toward the analysis of this challenging computational aeroacoustics problem.

1. Introduction

A detonation is an efficient process of converting stored chemical energy in fuels to useful thermal and mechanical energy for various applications. A PDE [1-5] is a novel propulsion concept based on the use of the high pressures generated by repetitive detonation waves in a thrust tube. In a typical PDE, the following process repeats itself over a frequency range of 40 to 150 Hz. First, the PDE tube is filled with a fuel/air mixture. The detonation is then initiated at the closed end of the thrust tube. The detonation wave propagates toward the tube exit, and the high-pressure region behind the detonation wave provides the thrust forces for the propulsion device. In the fully burned region immediately following the traveling shock wave, typical pressure rise is about 15 to 20 times of that in the unburned gases. We remark that the pressure peak of von Neumann spike could be 50 to 100 times of that seen in the unburned gases. However, this pressure peak is transient and does not produce useful thrust force.

Because the PDE tube is kept open at the tube exit throughout the fueling and firing process, pressure of the unburned gases is generally in equilibrium with the surrounding atmosphere. Moreover, because the flow is unconfined, the burned gases and the shock wave would travel at the sonic C-J velocity at the fully burned equilibrium condition.

Due to the traveling detonation wave, high pressures associated with the equilibrium condition in a ZND sense cannot be fully utilized. Following the detonation wave, the burned gases in the closed-end region expand and cause pressure reduction. Typically, pressure of the closed-end region during the firing process is only about 5 to 8 times of that in the unburned gases. This is the main source of the propulsion forces for a PDE.

Following the detonation wave, the pressurized burned gases leave the PDE tube and expand into the surrounding atmosphere. Due to the momentum of accelerating gases over-expansion occurs and expansion waves move forward and aft the PDE tube as well as into the PDE tube. As a result, pressure at the closed-end region reduces to be lower than that of the surrounding atmosphere.

---

1. Research assistant professor, Email: zhangzc@me1.eng.wayne.edu
2. Associate professor, Email: styu@me1.eng.wayne.edu
3. Ph.D. candidate, Email: haohe@me1.eng.wayne.edu
4. Aerospace engineer, Email: aejorgen@lerc.nasa.gov

This low-pressure condition inside the PDE tube is detrimental to propulsion, but could be useful in refueling the combustible mixture for the next firing. To ensure successful detonation initiation, experimentalists generally recommended purging the PDE tube by inert gas before refueling. By removing undesired combustion products as well as unsteady expansion/compression waves, the purging procedure refreshes the flow condition inside the tube, and thus avoids fuel leakage to the surrounding atmosphere.

In each firing cycle, gas blow-down and refueling processes occupy more than 90% of the time. A well-managed blow-down and refueling process is a key factor for continuous strong detonations and thus a successful PDE. During the detonation process, the shock wave travels at a supersonic speed with respect to the unburned gases, and the flow conditions outside the tube exit would have little impact to the traveling detonation wave. On the contrary, the blow-down and refueling processes strongly depend on the boundary conditions at the PDE exit, which in turn cannot be fully described without knowing details of the PDE plume dynamics. Consequently, to assess the performance of a PDE, we should simulate the PDE plume dynamics as an integral part of the overall calculation.

Moreover, because of pulsating jets, we anticipate significant pressure fluctuations in both forward and aft quadrants of a PDE. The main concern would be vibrations of the fuselage and wings of the aircraft due to periodic pressure loading. In addition, the acoustics distribution in the far field could be of concern. Typically in the past, computational aeroacoustics (CAA) for propulsion systems have been performed in a two-step approach: (1) CFD solution of the RANS equations for background mean flows at steady state, and (2) the solution of the linear wave equation for acoustic propagation. Because the background flow is highly unsteady with large flow structures, this approach is not appropriate in the present work. Simulation of the PDE plume dynamics is indeed a challenging CAA problem.

The objectives of the present paper are: (i) to conduct time-accurate CFD simulations of PDE plume dynamics based on reasonable operating conditions; and (ii) based on the numerical results, to understand the underlying flow physics of the unsteady PDE plumes. In the present work, we employ the space-time CE/SE method [6-11] for high-fidelity calculations of pulsating PDE plumes. In the future, based on the numerical results, we wish to propose remedies to suppress/deflect undesirable noises, and to study alternative blow-down and refueling processes for higher thrust output.

The rest of this paper is organized as follows: Section 2 presents the theoretical model equations to be solved. In Section 3, a brief description of the CE/SE method is provided. Section 4 provides numerical results and discussions of unsteady flows of single and multiple PDE tubes. We then offer concluding remarks and provide cited references.

2. The Model Equations

The axisymmetric Euler equations and one species equation are given as

$$\frac{\partial \mathbf{U}}{\partial t}+\frac{\partial \mathbf{F}}{\partial x}+\frac{\partial \mathbf{G}}{\partial y}=\mathbf{R}, \qquad (2.1)$$

where **U** is the unknown conserved flow variables, **F** and **G** are the flux vectors in axial and radial directions, and **R** is the source term vector for axisymmetric formulation and chemical reactions. Each column vector has five entries. Refer to Eqs. (2.2a) to (2.2d). In Eqs. (2.1-3), x and y are the axial and radial coordinates, respectively; ρ is density; u and v are the x- and y-component velocity; p is pressure; Z is the mass fraction of the reactant; and $E= e + Zq_o + (u^2+v^2)/2$ is the total energy with e as the sensible internal energy, and q_o the heat release due to chemical reaction.

$$\mathbf{U}=\begin{pmatrix} u_1 \\ u_2 \\ u_3 \\ u_4 \\ u_5 \end{pmatrix}=\begin{pmatrix} \rho \\ \rho u \\ \rho v \\ \rho E \\ \rho Z \end{pmatrix}, \qquad (2.2a)$$

$$\mathbf{F} = \begin{pmatrix} f_1 \\ f_2 \\ f_3 \\ f_4 \\ f_5 \end{pmatrix} = \begin{pmatrix} \rho u \\ \rho u^2 + p \\ \rho uv \\ (\rho E + p)u \\ \rho uZ \end{pmatrix}, \qquad (2.2b)$$

$$\mathbf{G} = \begin{pmatrix} g_1 \\ g_2 \\ g_3 \\ g_4 \\ g_5 \end{pmatrix} = \begin{pmatrix} \rho v \\ \rho uv \\ \rho v^2 + p \\ (\rho E + p)v \\ \rho vZ \end{pmatrix}, \qquad (2.2c)$$

$$\mathbf{R} = \begin{pmatrix} r_1 \\ r_2 \\ r_3 \\ r_4 \\ r_5 \end{pmatrix} = \begin{pmatrix} -\rho v / y \\ -\rho uv / y \\ -\rho v^2 / y \\ -(\rho E + p)v / y \\ -\rho vZ / y + \dot{\omega} \end{pmatrix}. \qquad (2.2d)$$

The chemical reaction is simulated by a global, one-step, finite-rate model with two chemical species, reactant and product. In the species equation, a source term $\dot{\omega}$ exists due to chemical reactions:

$$\dot{\omega} = -K\rho Z \exp(-E^+ / R_u T) \qquad (2.3)$$

where K is the pre-exponential factor of the Arrhenius kinetics, E^+ is the activation energy, R_u is the universal gas constant, an T is temperature. We assume that the gas mixture is polytropic, i.e., the molecular weights and the specific heats are constant for both unburned and burned gases. Note that the emphasis of the present work is the PDE plume dynamics. Because we anticipate little chemical reaction outside the PDE tube, a primitive finite rate model is used in the present work. In the actual calculations, the values of the constants in Eq. (2.3) are determined by simulating combustion of well-mixed propane/air gases.

3. The CE/SE Method

The space-time CE/SE Method, originally proposed by Chang [6,7,8], is a novel numerical framework for hyperbolic conservation laws. The CE/SE method is not an incremental improvement of a previously existing CFD method, and it differs substantially from well-established CFD methods. The CE/SE method has many non-traditional features, including a unified treatment of space and time in calculating flux conservation, the introduction of conservation element (CE) and solution element (SE), a novel shock capturing strategy without using a Riemann solver, and simple treatments for reflective, non-reflective, and no-slip boundary conditions based on a local space-time flux conservation over CEs near the computational boundaries [9]. Details of the CE/SE method have been extensively illustrated in the cited references [6-13].

To date, numerous highly accurate solutions have been obtained by the CE/SE method. Based on experience, we found that the CE/SE method is capable of capturing shocks and acoustic waves simultaneously, where the magnitude of the shock pressure jump could be several orders of that in the acoustic waves. The above high-resolution capabilities of the CE/SE method and the simple boundary condition treatment are critically important to the present calculations.

By applying the Gauss divergence theorem to Eq. (2.1) in a space-time domain, we obtain the following integral equation:

$$\int_{S(V)} \vec{h}_m \cdot d\vec{S} = \int_V r_m dV \text{ , } m=1,\ldots,5 \qquad (3.1)$$

where $\vec{h}_m = (f_m, g_m, u_m)$ is the space-time density flux, V is a space-time volume, and $d\vec{S}$ is a vector surface element of V, pointing outward. Numerical integration of Eq. (3.1) over V to balance the space-time flux locally and globally is the essence of the CE/SE method.

First, the space-time domain of interest is divided into solution elements (SEs). In each SE, flow variables are assumed continuous, and approximated by a first-order Taylor series. Thus the scheme is second-order accurate. Across the boundaries of neighboring SEs, flow discontinuities are allowed. Flow variables are marched forward in time by enforcing a local space-time flux balance over conservation elements (CEs), i.e., integrating Eq. (3.1) over CEs. Note that CEs are different from SEs, and in general various CEs could be employed for local and global space-time flux balance. We note that in the original CE/SE method, triangular and tetrahedron meshes in spatial domain are used.

Recently, the CE/SE method has been extended to include meshes of quads and hexes in two- and three-dimensional calculations [10,11]. The new solver can take unstructured quadrilateral meshes. In the present calculations, we used the extended CE/SE method with quadrilateral meshes.

In Eqs. (2.1) and (3.1), the source term is stiff in the sense that the time scale of chemical reactions is much smaller than that of convective fluxes. Previously, a splitting method [12] is developed to treat the stiff source term in the setting of the CE/SE method. The overall space-time flux balance over each CE is divided into the convection flux and the source. Calculation of convection flux is done in the manner without concerning the existence of the source term and is solely paced by the CFL constraint. The calculation of the source, on the other hand, is based on a space-time volumetric integration using smaller time increments. A backward difference method is used in integration for numerical instability and the scheme is locally implicit.

4. Results and Discussions

4.1 A Single Tube Thruster

Figure 4.1 shows the computational domain of a single tube thruster. The radius of the tube is 5 inches, and its length is 26.1 inches. At the beginning of each firing, 85% of the tube is filled with a propane/air mixture at an equivalence ratio of 1.3. The initial chamber pressure is 15 psia, and temperature is 510 R. The PDE tube is envisioned to operate at 60 Hz, i.e., 16.67 *ms* for one cycle.

Since the flow field is symmetric with respect to the thrust vector, the region above the symmetric line is used as the computational domain. The length and radius of the computational domain are 12.67 ft and 4.5 ft, respectively. The spatial domain is divided into 293,600 non-uniform quadrilateral cells, with clustering near the tube exit. Inside the PDE tube, a fine mesh is used, and the mesh size is 510×45.

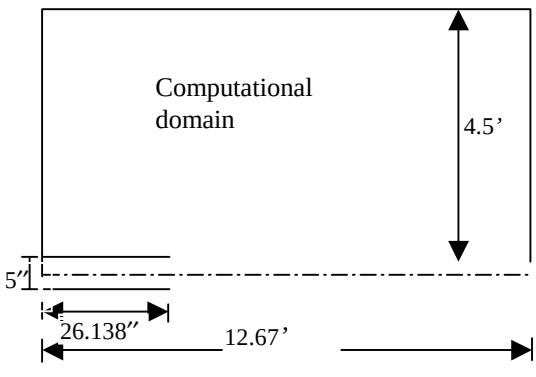

Fig. 4.1: The schematic of computational domain for a single tube and single firing condition.

When t=0, a one-dimensional analytical ZND solution is numerically mapped to the two-dimensional mesh near the closed end of the PDE tube [13]. Eight mesh nodes are used to resolve the flame zone of the prescribed ZND wave. After proper non-dimensionalization, the controlling parameters of the detonation wave are the overdriven factor f, the specific heat ratio γ, the activation energy E^+, and the heat release rate q_o. Refer to Eq. (2.3). In the present calculation, the C-J detonation is anticipated. Thus f =1.0. The other parameters are

$$\gamma=1.2015,\ E^+=37.56,\ q_o=35 \qquad (4.1)$$

In the setting of the simplified combustion model employed in Eq. (2.3), the above data were deduced by comparing the equilibrium calculations (NASA CEA program [14]) to the known flow conditions for propane/air detonation.

The detonation wave is ignited at the closed end of the thrust tube, and travels from left to right. Figure 4.2 shows the time history of pressure at the closed end of the thrust tube for single tube and single pulse firing condition. When the detonation is initiated at the closed end, there is a big pressure jump up to about 17.235 bars, which is the equilibrium C-J pressure of the propane/air detonation.

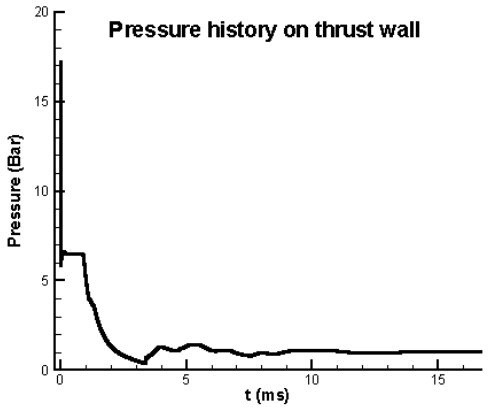

Fig. 4.2: Time history of pressure at the closed end of a propane/air thrust tube for a single tube and single pulse firing condition.

The high pressure, however, is sustained for only a very short period of time due to the induced flow expansion behind the traveling detonation wave.

Pressure at the closed end quickly reduces to only about 6.5 bars, and maintain that constant level until the reflected expansion wave reaches the closed end of the PDE tube at about t = 0.9 *ms*. Although 0.9 *ms* is less than 6% of one cycle (16.67 *ms*), it is the time period when the PDE tube is producing thrust forces. Further examination showed that it takes only about 0.361 *ms* for the detonation wave to travel through the tube. Thus, it takes about 0.54 *ms* for the expansion wave to reach the closed end of the tube after the detonation wave has left the PDE tube. The time during which the detonation wave is traveling inside the PDE tube is only about 2 percent of a PDE cycle (16.67 *ms*).

After the expansion wave has reached the closed end of the PDE tube, pressure declines steeply. When t = 3.4 *ms*, the pressure at the closed-end of the tube reaches its lowest value, less than half of the atmospheric pressure. This is the ideal time to begin the refueling/purging process for the next firing cycle.

From 3.4 *ms* to about 10 *ms*, the closed-end pressure fluctuates with significant amplitude, roughly 0.5 bar at the initial stage and asymptotically approaching the atmospheric level as time evolves. These pressure fluctuations are the result of complex vortex/shock interactions outside of the detonation tube, and they are detrimental to the refueling and purging process.

Figure 4.3 shows three snapshots of the pressure contours after the detonation wave has exited the thrust tube. The detonation wave quickly quenches and becomes a non-reactive shock wave. The pressurized gases near the PDE tube exit quickly expand in a spherical manner forward and aft of the PDE tube. The expansion wave also travels upstream into the PDE tube. In [5], Wilson and Paxson have proposed a heuristic and insightful theoretical model for the PDE plume dynamics. In their model, the authors eloquently pointed out the spherical expansion wave as the final stage of the PDE plume expansion. The present CFD results strongly support their proposed model.

Figure 4.4 illustrates the vortex/shock interactions in the near field. Due to a strong jet, a vortex ring is developed outside of the PDE tube. The vortex ring functions as a convergent/divergent nozzle. The jet accelerates to be supersonic through this fluid nozzle. Shown in Fig. 4.4 (a), the supersonic jet is adjusted to the surrounding air through a bow shock. In Fig. 4.4(a), the shock wave stands on the divergent section of the fluid nozzle. At a later stage of the wave expansion, due to decreasing mass flow rate, the vortex ring shrink in radius and the fluid nozzle closes at its exit. In this transient process, the shock wave would occasionally stand on the converging section of the fluid nozzle. Under this condition, the jet behaves just like an un-started inlet and the shock wave travels quickly upstream into the PDE tube.

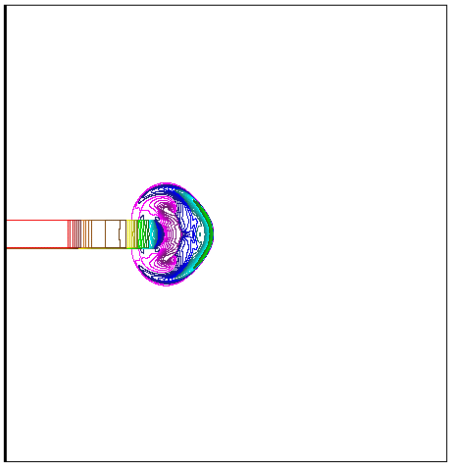

(a) t = 0.642 *ms*

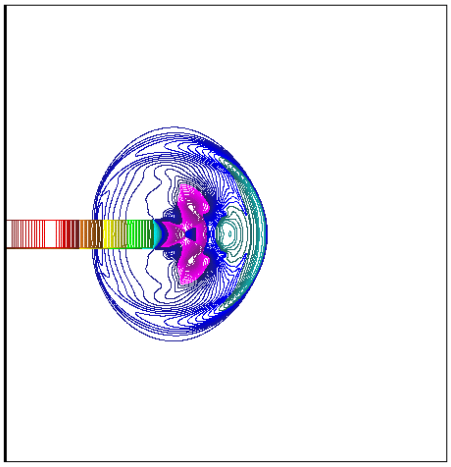

(b) t = 1.124 *ms*

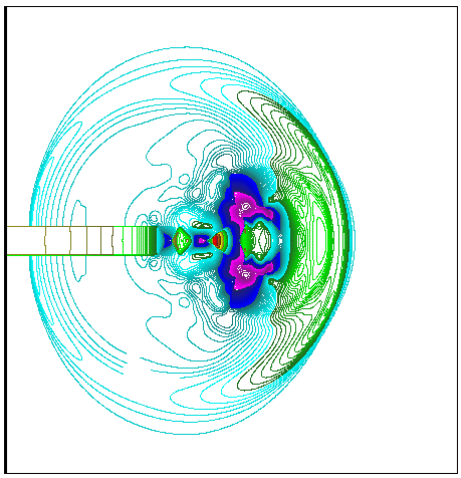

(c) t = 1.927 *ms*

Fig 4.3: Three snapshots of pressure contours of a PDE plume at the initial stage of expansion.

The above discussions illustrated the mechanism responsible for the alternating expansion and compression waves experienced by the closed end of the PDE tube from 3.4 to 10 *ms* as shown in Fig. 4.2.

Figure 4.5 shows pressure histories at two different locations outside the tube exit. One dominant pressure peak occurs when the primary shock wave reaches the location. Following the shock wave, a pressure dip exists. Further downstream and away from the PDE tube, the nonlinear pressure wave dissipates and become a weak sound wave, propagating in a spherical manner to the far field. Refer to the Wayne State CFD web site cfd.eng.wayne.edu for more information about acoustic propagation of this PDE. Figure 4.6 shows the time histories of pressure and density at a near field location inside the PDE plume. Here pressure trace shows little variations from one cycle to the other. However, time history of density shows significant cycle-to-cycle variations.

4.2 A PDE with Three Detonation Tubes

In this section, a hypothetical 3-tube PDE is of concern. Figure 4.7 shows the schematic for the computational domain. Note that all the length scales are dimensionless with half of the distance between neighboring tubes as the reference dimension. The computational domain is divided into 214,800 uniform cells. The flow conditions are:

$$\gamma=1.2,\ E^{+}=50,\ q_o=50 \qquad (4.2)$$

The initial detonation waves are located at x = 15, 5, and 15 in tubes *a*, *b* and *c*, respectively. The one-dimensional ZND analytical solution is used as the initial condition. Figure 4.8 shows three consecutive snapshots of the pressure contours. Detonation

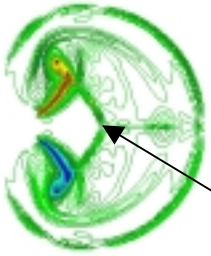

(a)

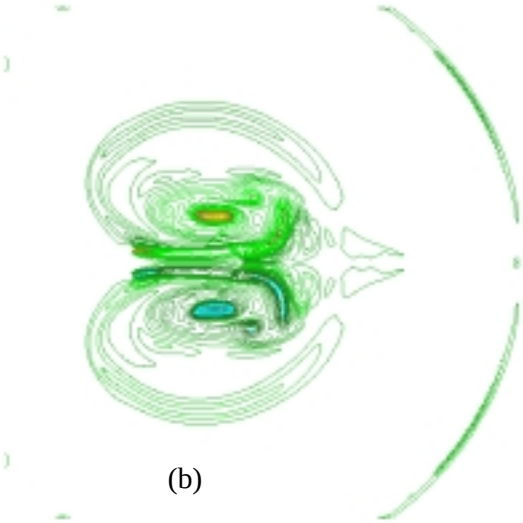

(b)

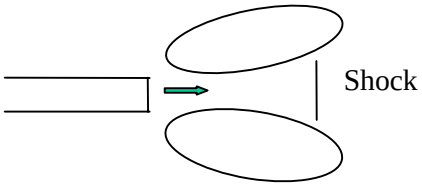

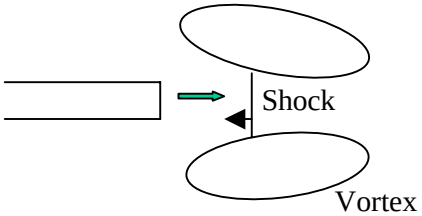

waves first exit from tubes (*a)* and (*c)*. As seen in the single tube case, the expanding shock waves are spherical. At a later stage, the shock wave coming from the central tube (b) interrupts expansion waves from (a) and (c). Eventually, a new and bigger spherical wave is formed. Because of the interacting shocks from different thrust tubes and the reflected waves from solid wall, the flow pattern is very complex. The expansion/compression flow pattern as that illustrated in Fig. 4.4 cannot be applied to this complex flow condition.

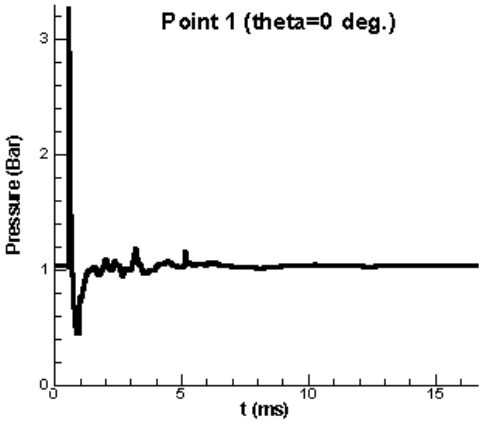

(a)

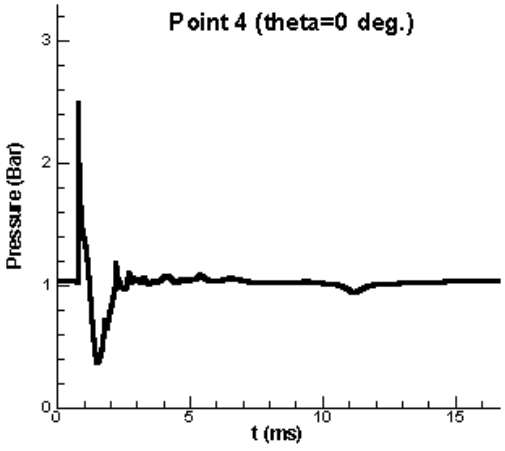

(b)

Fig. 4.5: Time histories of pressures at two locations: (a) (4.11”, 0.49’) and (b) (11.329”, 0.49’). The coordinates are measured by using the center of the PDE tube exit as the origin.

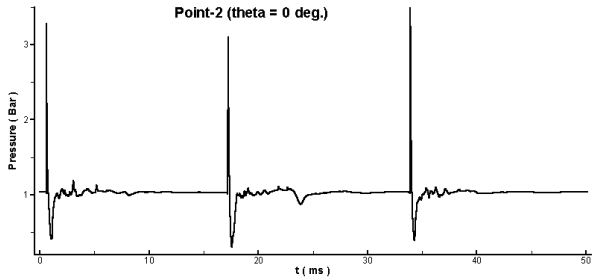

(a)

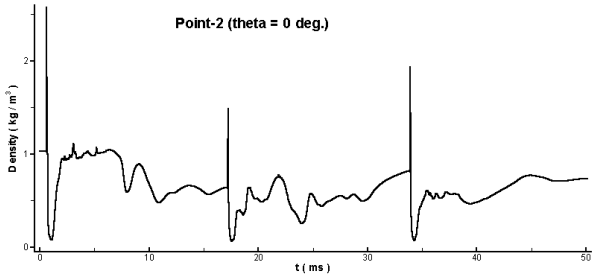

(b)

Fig. 4.6: Time histories of pressures and density at the location (5.66 inches, 0.49 ft) for a three cycle calculation. The coordinates are measured by using the center of the PDE tube exit as the origin.

Fig. 4.7: The schematic of the computational domain for a three-tube PDE plume calculation.

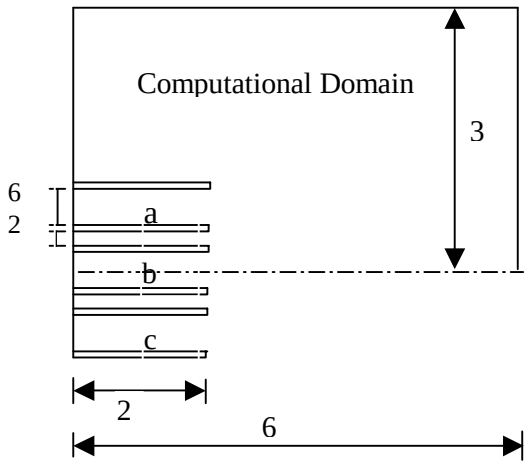

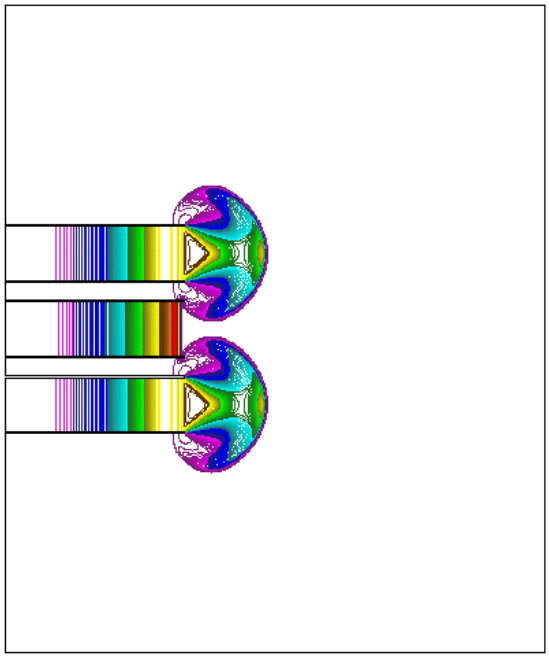

(a)

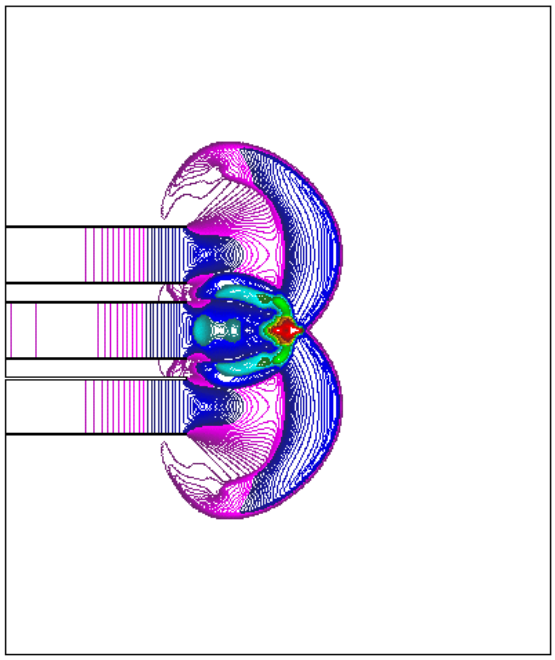

(b)

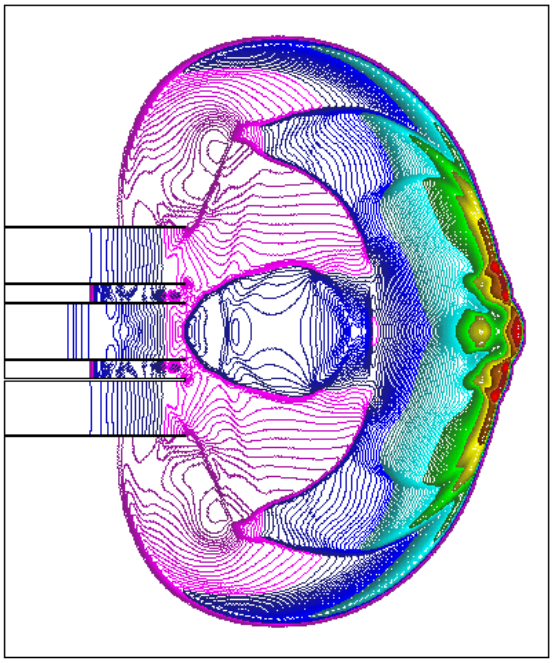

(c)

Fig. 4.8: Three snapshots of pressure contours of a three-tube PDE.

Concluding Remarks

In the present paper, the CE/SE method has been employed to study the complex plume dynamics of a propane/air PDE. Preliminary numerical results were demonstrated, including a single tube PDE with a single pulse firing and three consecutive pulses firing, and a three-tube PDE with a single pulse firing. The flow condition was chosen to mimic realistic PDE operating conditions. Numerical results show that in about 6% of a PDE cycle, the engine is actively producing thrust forces. The time for traveling detonation wave through the PDE tube is less than 3% of one cycle. The rest of the time is occupied by the blow-down and refueling processes, which heavily depend on the flow conditions outside of the PDE tube. Outside the PDE tube, flow expands and accelerates through a vortex ring, which behaves like a fluid funnel. Due to unsteadiness of the shock/vortex interactions, alternating expansion and compression occur in the near field of the PDE plume. Away from the PDE tube, a spherical expansion is the dominant flow feature for both single tube and three tube cases.

Numerical results by the CE/SE method show all salient features of complex shock/shock and shock/vortex interactions. Many fine flow features are crisply resolved. More information and animated results could be viewed on our web page: cfd.eng.wayne.edu. All results shown in the present paper were obtained by using a desktop PC with one Pentium III CPU. Further investigations using finer meshes and parallel computers are needed to further resolve the complex flow features.

Acknowledgement

The second author of the present paper wishes to acknowledge fruitful discussions with C.L. Merkle of Univ. of Tennessee, K. Kailasanath of NRL Navy, J.-L. Cambier of MSE in Montana, F. Schauer of WPAFB Air Force, and J. Wilson of NASA Glenn. The present work has been sponsored by NASA Glenn, monitored by D. Perkins and R. Blech.

References

1. K. Kailasanath, G. Patnaik and C. Li, "Computational Studies of Pulse Detonation Engines: A Status Report," AIAA 99-2634 (1999).

1. C.P. Li, K. Kailasanath and G. Patnaik, "A Numericaal Study of Flow Field Evolution in a Pulsed Detonation Engine," AIAA paper 2000-0314 (2000).

2. K. Kailasanath, "A Review of PDE Research: Performance Estimates," AIAA 2001-0474 (2001).

3. H.B. Ebrahimi, R. Mohanraj, and C.L. Merkle, "Multi-Level Analysis of Pulse Detonation Engine," AIAA Paper, 2000-3589 (2000).

4. F. Schauer, J. Stutrud, and R. Bradley, "Detonation Initiation Studies and Performance Results for Pulse Detonation Engine Applications," AIAA Paper 2001-1129 (2001).

5. J. Wilson and D. E. Paxson, "On the Exit Boundary Condition for One-dimensional Calculations of Pulsed Detonation Engine Performance," the 18th International Colloquium on the Dynamics of Explosions and Reactive Systems, July 29th -August 3, 2001, Seattle, Washington.

6. S. C. Chang, The Method of Space-Time Conservation Element and Solution Element – A New Approach for Solving the Navier Stokes and Euler Equations, *J. Comput. Phys*., 119 (1995) p. 295

7. S.C. Chang, X.Y. Wang and C.Y. Chow, The Space-Time Conservation Element and Solution Element Method: A New High-Resolution and Genuinely Multidimensional Paradigm for Solving Conservation Laws, *J. Comput. Phys.*, 156 (1999) p. 89.

8. S. C. Chang, X. Y. Wang and W. M. To, "Application of the Space-Time Conservation Element and Solution Element Method to One-Dimensional Convection-diffusion Problems," *J. Comput. Phys.*, 165, 189 (2000).

9. S.C. Chang, A. Himansu, C. Y. Loh, X. Y. Wang, S.T. Yu, P. Jorgenson, Robust and Simple Nonreflecting Boundary Conditions for the Space-Time Conservation Element and Solution Element Method, AIAA Paper 97-2077 (1997).

10. Z. C. Zhang and S. T. Yu, Shock Capturing without Riemann Solver — A Modified Space-Time CE/SE Method for Conservation Laws, AIAA Paper 99-0904 (1999).

11. Z.C. Zhang, S.T. Yu, S.C. Chang, A. Himansu and P. Jorgenson, A Modified Space-Time CE/SE Method for Euler and Navier-Stokes Equations, AIAA Paper 99-3277 (1999).

12. S.T. Yu and S.C. Chang, "Treatments of Stiff Source Terms in Conservation Laws by the Method of Space-Time Conservation Element and Solution Element," AIAA Paper 97-0435 (1997).

13. Z.C. Zhang, S.T.J. Yu, H. He, S.C. Chang, "Direct Calculations of Two- and Three-Dimensional Detonations by an Extended CE/SE Method," AIAA 2001-0476 (2001).

14. B. J. McBride and S. Gordon, "Computer Program for Calculation of Complex Equilibrium Compositions and Applications," NASA Reference Publication 1311, NASA Lewis Research Center (1996).